Development of Cerebella Tissue of Rat Characterized by Acoustic Impedance Microscope

N.Hozumi
Aichi Inst. of Technology
Toyota, Japan
hozumi@aitech.ac.jp

A. Kimura, S. Terauchi, M. Nagao, S. Yoshida
Toyohashi Univ. of Technology
Toyohashi, Japan

K. Kobayashi
Honda Electronics Co., Ltd.
Toyohashi, Japan

Y. Saijo
Tohoku Univ.
Sendai, Japan

***Abstract*— Acoustic microscopy is expected to be a powerful tool for observing biological matters without chemical staining. We have proposed a new method for two-dimensional acoustic impedance imaging for biological tissue that can perform micro-scale observation without preparing a sliced specimen. A tissue was attached on a 0.5 mm-thick plastic substrate. An acoustic pulse was transmitted from the rear side of the substrate. The reflection intensity was interpreted into local acoustic impedance of the target tissue. In the previous report, we demonstrated the outline of the system and the result of preliminary observation, showing its feasibility. This report deals with the optimization of the observation method, and characterization of the tissue of developing cerebellum. The result shows that change in acoustic impedance of each cerebellar layer depending on postnatal day was correspond to change of structure with growth.**

Keywords: biological tissue; acoustic impedanc; micro-scale imaging.

I. INTRODUCTION

Optical microscopy of biological tissue is generally taken after slicing and staining the tissue. This is destructive both mechanically and chemically. In addition, it needs relatively long time for staining process. On the contrary, acoustic imaging can be performed without staining process; i.e., it is chemically non-destructive. The observation can be finished in a very short time, as it does not need staining process. The idea of ultrasonic microscopy for biological tissue is based on this advantage, and it is considered to become a powerful tool for tissue characterization that can image elastic parameters.

Most of ultrasonic microscopes are scanning type, in which the response to a focused acoustic signal is successively acquired as the beam is mechanically scanned[1,2].The authors previously proposed a pulse driven ultrasonic sound speed microscopy that can obtain sound speed image in a short time [3,4]. Although a small roughness of the specimen was approved in this type of microscope, slicing the specimen into several micrometers was still required for the observation. However it is often required that the observation can be performed without slicing process, as slicing may damage some functions of a tissue.

Based on the above background, the authors have proposed the acoustic impedance microscopy that can image the local distribution of cross-sectional acoustic impedance of tissue[5]. As acoustic impedance is given as a product of sound speed and density, it would have a good correlation with sound speed, when the variance in density was not significant. In the previous report, the methodology of micro-scale imaging of cross-sectional acoustic impedance and its accuracy was described, showing its feasibility. In this report, the efforts to upgrade the image quality are dealt with. Thanks to these effort, a satisfactory clearness and precision of the image was realized. As an example, the change in postnatal day of each layer of cerebellum tissue of a rat was quantitatively characterized.

II. SAMPLE PREPARATION

The cerebellum tissue of a rat was employed as the specimen to be observed. Rats were dissected and removed their whole brains. To role out the effects of cross linker on the identification of neuronal structures by their acoustic impedance, we observed fresh cerebella organs without any chemical fixation. A sagittal cross section was exposed by a rotor slicer (Dohan EM, Kyoto, Japan). The specimen was rinsed and preserved in the same phosphate buffer solution (PBS). For optical observation, some adjacent slices were subjected to immunohistochemical staining against calbindin D-28k.

III. EXPERIMENTAL SETUP

Figure 1 illustrates the outline of the acoustic impedance microscope [5,6]. The tissue was attached on a 0.5 mm-thick plastic substrate. Distilled water was used as a coupling medium between the substrate and transducer. A sharp electric pulse of about 40 V in peak voltage and 2 ns in width was generated by the pulse generator (AVTEC, AVP-AV-HV3-C). The transducer was PVDF-TrFE type. An acoustic wave with a wide frequency range was generated by applying the voltage pulse. The acoustic wave, being focused on the interface between the substrate and tissue, was transmitted and received by

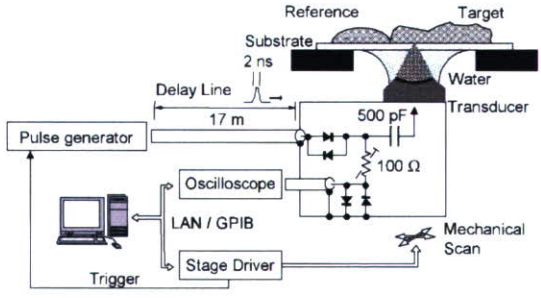

Fig.1 Schematic diagram of the system.

the same transducer. Considering the focal distance and the sectional area of the transducer, the diameter of the focal spot was estimated as about 40 μm at 80 MHz.

The substrate was a flat plastic plate made of polymethylmetacrylate (PMMA), its thickness being 0.5 mm. In order to retain hydrophilic property of the substrate, the surface was subjected to a plasma treatment using Keyence ST-7000. A reference material, of which acoustic impedance was known, was also placed on the same substrate. In many cases, the target tissue was observed together with the reference, by including it in the same field of view. In this series of experiment, we used pure water or a silicone rubber as the reference material. The substrate pasted with the rubber was preserved more than 12 hours after the rubber had been cured.

The reflection was detected and digitized by the oscilloscope (Tektronix, TDS-7145B). Two-dimensional profile of acoustic impedance was obtained by mechanically scanning the transducer. A typical field of view of 4 mm x 4 mm was covered with 200 x 200 pixels. It took typically 2 - 3 minutes for one observation. All the measurements were performed at room temperature.

The target signal is compared with the reference signal and interpreted into acoustic impedance as

$$Z_{target} = \frac{1-\frac{S_{target}}{S_0}}{1+\frac{S_{target}}{S_0}} Z_{sub} = \frac{1-\frac{S_{target}}{S_{ref}} \cdot \frac{Z_{sub}-Z_{ref}}{Z_{sub}+Z_{ref}}}{1+\frac{S_{target}}{S_{ref}} \cdot \frac{Z_{sub}-Z_{ref}}{Z_{sub}+Z_{ref}}} Z_{sub}$$

where S_0 is the transmitted signal, S_{target} and S_{ref} are reflections from the target and reference, Z_{target}, Z_{ref} and Z_{sub} are the acoustic impedances of the target, reference and substrate, respectively [5,6].

In case of using water as the reference, its acoustic impedance was assumed to be 1.5 x 10^6 Ns/m^3. On the other hand, in case of using silicon rubber, the acoustic impedance of itself was calibrated, by using water as the standard reference material. In this report, 0.965 x 10^6 Ns/m^3 was used. The acoustic impedance of the substrate was calculated to be 3.22 x 10^6 Ns/m^3,considering its sound speed and density.

IV. RESULTS AND DISCUSSION

A. Observation of cerebellar cortex of a rat

Figure 2 illustrates the development of cerebellar cortex. In immature cerebellum, structure of layer is not clear, but in mature cerebellum, 4 layers are visible; molecular layer (ML), Purkinje layer (PL), internal granular layer (IGL) and white matter (WM). Parallel fibers in ML are axon of granule cells and play an important role in cerebella neural connection. Migrating granule cells elongate them horizontally and form a lot of excitatory synapses to dendrite of Purkinje cells. These are major neuronal circuits of cerebellum so that parallel fibers are expected to construct rich ML with development.

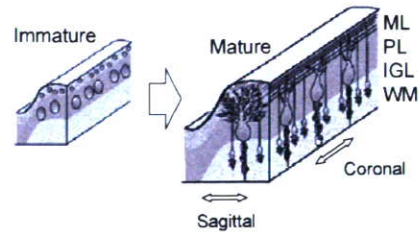

Fig. 2 Illustration of development of cerebellar cortex.

In order to upgrade the clearness and precision of the acoustic impedance image, we took following two countermeasures;

(1) Surface of the substrate was treated with plasma to upgrade hydrophilic property.
(2) The specimen was kept in humid condition during the measurement, using a protection cover mounted on the substrate.

B. Plasma treatment

The PMMA substrate was chosen, as it has a good accuracy of dimension and acoustic transmittance. However, its hydrophilic property is not sufficient, leading to a poor contact between the substrate and tissue. Figure 3 shows the images with and without plasma treatment for the substrate surface. The images were taken from the rats of the same postnatal day.

In image (a), although the layers close to the boundary between the tissue and outside (the part that looks black in the image) are clearly seen, those inside the tissue are not clear. This would be due to a coupled water layer to the tissue on the substrate. In order to improve the contact by upgrading hydrophilic property, a plasma treatment was performed prior to the observation. After plasma treatment, a contact angle to water reduced from 55 degrees to 39 degrees. Surface energy after plasma treatment would be increased, bringing about a better hydrophilic property. As its good hydrophilic property is kept for about one hour, the observation was completed within one hour after the treatment. As shown in image (b), the internal structure is clearly seen when the treatment was performed.

In order to quantitatively assess the effect of plasma treatment, the acoustic impedance through the same layer was traced. Figure 4 shows the examples. Each trace was performed along the white line indicated in Figure 3. The acoustic impedance of ML, as its fine structure made with a fat sheath

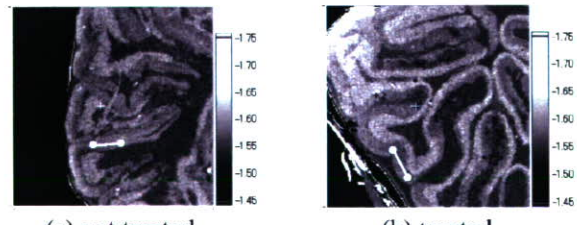

(a) not treated (b) treated

Fig.3 Effect of plasma treatment.

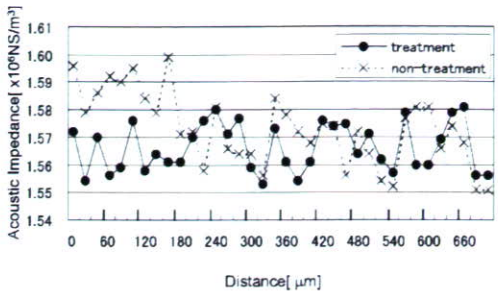

Fig.4 Change of acoustic impedance along the white line indicated in Fig. 3.

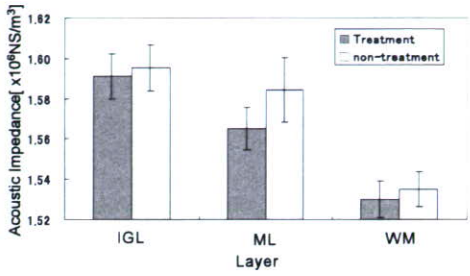

Fig. 5 Acoustic impedance of each layer with and without plasma treatment.

of myelin is far less than the scale of focal spot, should be uniformly observed. However as shown in the figure, a significant difference in dispersion is seen depending on the surface condition of the substrate. It is obvious that the ML is observed with more uniform acoustic impedance by treating with plasma.

Figure 5 shows the acoustic impedance of each layer with and without plasma treatment. Each bar represents the average of 400 points, the length of error bar indicating twice the standard deviation. Plasma treatment does not seem to affect the acoustic impedance of IGL and WM, both in average and standard deviation.

On the other hand, in case of ML, there is a difference of 0.022×10^6 Ns/m^3 in average acoustic impedance, as well as a significant difference in standard deviation. This would result from the structure of each layer. A lot of fine fibers are assembled in ML, whereas both WM and IGL are formed from coherent large cells. An ML fiber, 0.2 micrometers in diameter, is much smaller than the cell scale of WM and IGL ranging from ten to a few tens of micrometers. Cell surface shows both hydrophilic and hydrophobic properties, though it is coupled with hydrating water molecules in solution. Most cells could contact with the hydrophobic substrate without hydrating water. Even if the substrate gets more hydrophilic property by plasma treatment, large cells composing WM and IGL could exclude surface water, leading to a relatively firm contact with the substrate. Therefore acoustic impedance of these layers did not show a significant variation depending on the plasma treatment.

However, in the case of ML, the fine fibers might be too small to tightly contact with the substrate. When the substrate acquires hydrophilic property, water could move thorough the ML and form a water-rich layer in contact with the substrate. Therefore the ML on the substrate after plasma treatment would indicate a lower acoustic impedance, reflecting the low acoustic impedance of water. Furthermore, this water-rich layer would bring about relatively low standard deviation in acoustic impedance compared with the case without the plasma treatment.

C. *Prevention from dry out*

The tissue specimen tend to dry out, leading to higher acoustic impedance. Figure 6 (a) shows this problem. The images of the tissue observed shortly after the preparation is shown in the left side. When the specimen had been exposed to the air with 22 % of relative humidity at 38 C for 20 minutes, the image was significantly changed as shown in the left side image. In order to prevent the dry out, a protection cover, as shown in Fig. 7, was mounted on the substrate after sample preparation. As shown in image (b), the change of image due to dry out was sufficiently prevented by applying the protection cover.

In order to confirm its effectiveness, a droplet of 2 wt% saline solution was subjected to the observation at 23 C in 56 % of ambient relative humidity, using pure water as the reference.

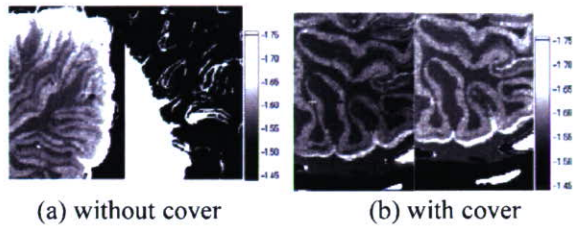

Fig.6 Acoustic impedance images shortly after mounting the tissue on the substrate (left) and 20 minutes later (right).

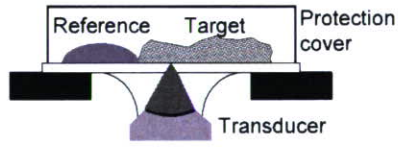

Fig.7 A protection cover mounted on the substrate.

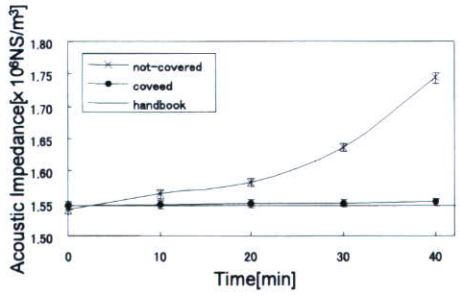

Fig.8 Change in time of acoustic impedance of saline droplet placed on the substrate. Initial content of NaCl was 2 wt%.

Figure 8 shows the result. Each plot represents the average of 900 points, the length of error bar indicating twice the standard deviation. The dotted line represents the acoustic impedance calculated from the handbook data. In case without the cover, due to concentration, the change of impedance is not negligible at 10 minutes, and it reaches as high as 1.75 x 10^6 Ns/m^3 at 40minuites. This change is not erroneous, as the precision of this measurement is proved to be as small as 0.006 x 10^6 Ns/m^3[5]. On the contrary, in case with the protection cover, the acoustic impedance is measured as a constant value not depending on time. It is supposed that the saturated humidity inside the cover successfully protected from dry out.

D. *Acoustic impedance of each layer of cerebellum depending on its development*

Figure 9 shows the observed images of cerebellar cortex of rat at immature (P1: postnatal 1 day), transient (P7 and P14), and mature (p21) stages. In the immature cerebellar cortex (P1), the external granular layer (EGL), the outer layer of the cortex, showed higher impedance than the inner layers. At this stage, many stiff granule cells compose EGL. In the inner layers, myelination is not yet progressed, and the existence of white matter is not clearly observed.

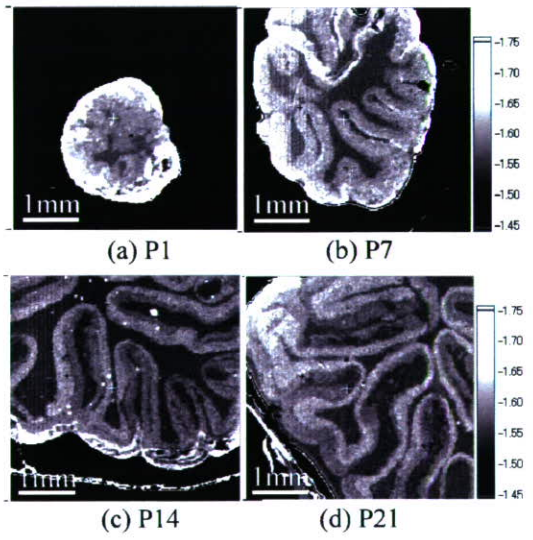

Fig.9 Two-dimensional profiles of acoustic impedance of cerebellar cortex.

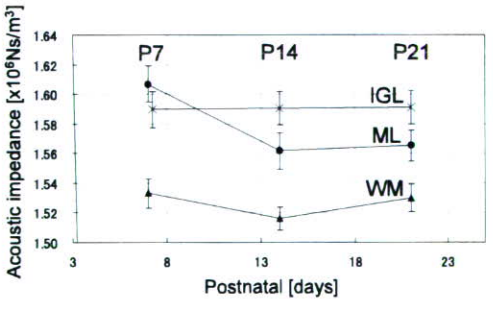

Fig 10 Change of acoustic impedance of each layer as a function of postnatal day.

Over transient stage, four different layers are clearly observed. As shown in Fig. 10, acoustic impedance of ML indicated higher value once in P7, but it decayed through the growth up to P14. The IGL is kept at high impedance, and the WM is kept at low. It is suggested that migrating granule cells in ML lead to a high impedance in P7, and relatively stable impedances of IGL and WM would be reflected from the stable properties of these layers.

V. Conclusions

Acoustic impedance microscope for biological tissue characterization was proposed. It can perform the observation neither staining nor slicing the specimen. Two measures to upgrade the image quality were taken. Plasma treatment improved the hydrophilic property of the substrate surface. Protection cover was proved to keep the specimen in good condition for observation. A quantitative assessment of acoustic impedance of each layer of cerebellar tissue in the development process of a rat was performed without chemical fixation. IGL and WM showed relatively stable value, whereas a significant change as a function of postnatal day was seen with ML. The change in acoustic impedance of ML would be reflecting the development of parallel fiber structure.

Acknowledgements

The authors would like to express their sincere thanks to T. Morishima and E. Fukushi of Toyohashi University of Technology for their assistance with the experiment. This study was financially supported by Grants-in-Aid for Scientific Research (Scientific Research (B)18360196), and Japan Society for the Promotion of Science and Health and Labor Sciences Research Grants from the Ministry of Health, Labor and Welfare for the Research on Advanced Medical Technology (H17-Nano-001).

References

[1] Y. Saijo, M. Tanaka, H. Okawai, H. Sasaki, S. Nitta & F. Dunn: "Ultrasonic Tissue Characterization of Infarcted Myocadium by Scanning Acoustic Microscopy", *Ultrasound in Med. & Biol.*, 23-1, 77 (1997).

[2] H. Okawai, K Kobayashi & S. Nitta: "An Approach to Acoustic Properties of Biological Tissues Using Acoustic Microgfraphs of Attenuation Constant and Sound Speed", *J. Ultrasound Med.*, 20, 891 (2001).

[3] N. Hozumi, R. Yamashita, C-K Lee, M. Nagao, K. Kobayashi, Y. Saijo, M. Tanaka, N. Tanaka & S Ohtsuki: "Ultrasonic Sound Speed Microscope for Biological Tissue Characterization Driven by Nanosecond Pulse", *Acoustic Science & Technology*, 24, 386 (2003).

[4] N. Hozumi, R. Yamashita, C-K. Lee, M. Nagao, K. Kobayashi, Y. Saijo, M. Tanaka, N. Tanaka & S.Ohtsuki: "Time –frequency analysis for pulse driven ultrasonic microscopy for biological tissue characterization", *Ultrasonics*, 42, 717 (2003).

[5] N. Hozumi, A. Kimura, S. Terauchi, M. Nagao, S. Yoshida, K. Kobayashi & Y. Saijo: "Acoustic Impedance Micro-imaging for Biological Tissue Using a Focused Acoustic Pluse with a Frequency Range Up to 100 MHz" IEEE International Ultrasonics Symposium, pp170-173 (2005).

[6] A. Kimura, N. Hozumi, S. Terauchi, M. Nagao, S. Yoshida, K. Kobayashi & Y. Saijo: "Imaging for Biological Tissue with Acoustic Impedance Microscope", 8th sendai symposium on Ultrasonic Tissue Characterization (2005).

Classification of Flow-limiting Thrombus in Acute Coronary Syndromes by High-frequency Acoustic Microscopy

Hidehiko Sasaki, Takayuki Kanno
Miyagi Cardiovascular and Respiratory Center
Kurihara, Japan

Yoshifumi Saijo, Motonao Tanaka
Institute of Development, Aging and Cancer, Tohoku University
Sendai, Japan

***Abstract*— Background: Virtual Histology- intravascular ultrasound (VH-IVUS) has the ability to help us distinguish between stable and unstable coronary plaques, but provides a limited definition of vulnerability on a size scale less than 100 m. The purpose of this study is to identify the acoustic properties of flow-limiting thrombus responsible for acute coronary syndromes(ACS) at the microscopic level. Methods: Acoustic microscopy operating in the high frequency range was used to display the two-dimensional distributions of color-coded images of attenuation and sound speed. A total of 26 cases of ACS patients were investigated. The tissues were sectioned at 5 mm thickness and mounted onto glass slides, were neither covered by slips nor stained. Results: The values of attenuation constant and sound speed for the red-thrombus were significantly higher than those for the platelets-rich thrombus. Both acoustic parameters for old red-thrombus were significantly lower than those for the organized thrombus. Conclusions: The acoustic properties of the flow-limiting thrombus at different stages of pathology can be classified by high-frequency acoustic microscopy. These criteria will hopefully provide a information regarding the development of a new IVUS.**

Keywords-acute coronary syndrome; thrombus; acoustic microscopy; attenuation; sound speed

I. INTRODUCTION

Virtual Histology- intravascular ultrasound (VH-IVUS) can distinguish stable and unstable coronary plaques, but it provides limited information on thrombus in coronary atherosclerosis. The purpose of this study is to clarify the acoustic properties of coronary thrombi at the microscopic level.

II. METHOD

A. Sound Speed Acoustic Microscopy

A SAM system specially developed in Tohoku University, operating in the frequency range of 50-150 MHz, was used for this study [1-6]. The sections for SAM measurements were mounted on glass slides but not covered by cover slips. The paraffin was removed from the sections by the graded alcohol method prior to the ultrasonic measurement. Distilled water was used as the coupling medium, which maintained the specimen at 20°C during the measurement procedure. A single ultrasound pulse of 5 ns width was emitted and received by the same transducer above the specimen. The reflection from the tissue surface and that from the interface between the tissue and glass were introduced into a personal computer using a high-speed A/D converter (DP210, Acqiris, Switzerland). The sampling speed was 2 GSa/s and the resolution was 8-bit. Eight values of the time taken for a pulse response at the same point were averaged in order to reduce the noise in the measurement. The transducer was mounted on an X-Y stage with a microcomputer board that was controlled by the personal computer. Both X-scan and Y-scan were driven by linear servo motors. The area of measurement was 2.4x2.4 mm with 300x300 pixels.

Figure 1 is the block diagram of the sound speed microscopy.

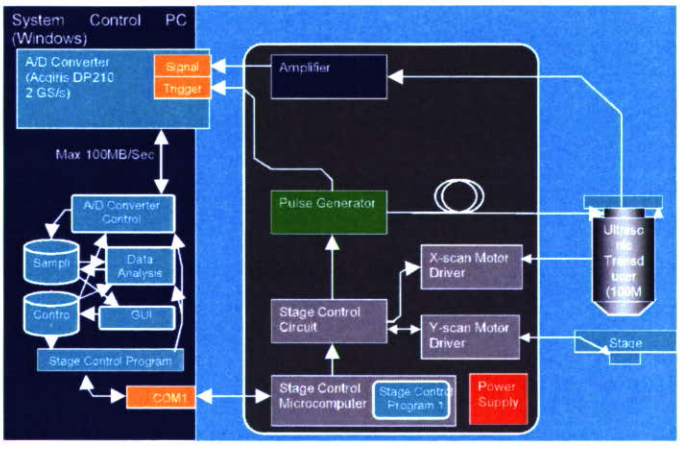

Figure 1. Block diagram of the sound speed microscopy

B. Sample for Measurement

Thirty-nine patients with coronary artery disease who received percutaneous coronary intervention were investigated. Tissues were retrieved from the coronary artery by aspiration catheter system (Thrombuster®) or directional coronary atherectomy procedures. The tissues for acoustic microscopy were fixed by 10% formalin, sectioned at 4 μm thickness and mounted onto glass slides without cover slips or staining. A neighboring section of the specimen was stained with Elastica-masson staining and observed by light microscopy. Figure 2 shows the appearance of the thrombus aspiration catheter system. Figure 3 shows the aspirated thrombus by the system.

Figure 2. Apperance of thrombus aspiration cathter

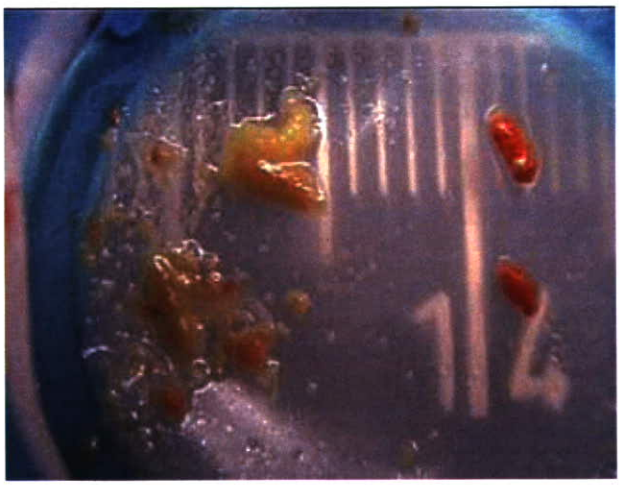

Figure 3. Aspirated thrombus

III. Results

Figure 4 is the optical (upper), attenuation (middle) and sound speed (lower) images of the thrombus 50 hours after AMI onset.

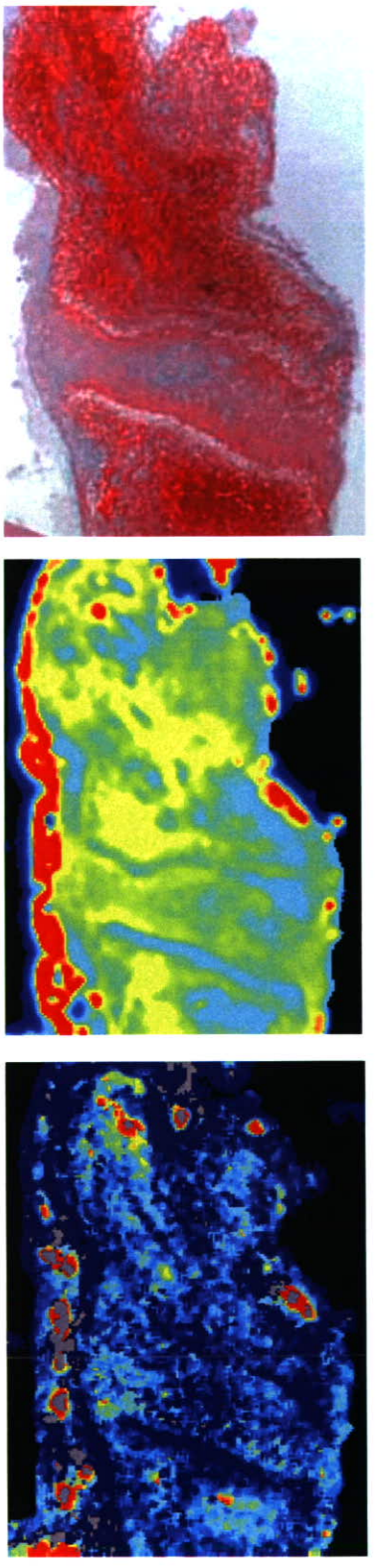

Figure 4. Optical (upper), attenuation (middle) and sound speed (lower) images of the thrombus 50 hours after AMI onset.

Figure 5 is the optical (upper), attenuation (middle) and sound speed (lower) images of the thrombus 19 hours after AMI onset.

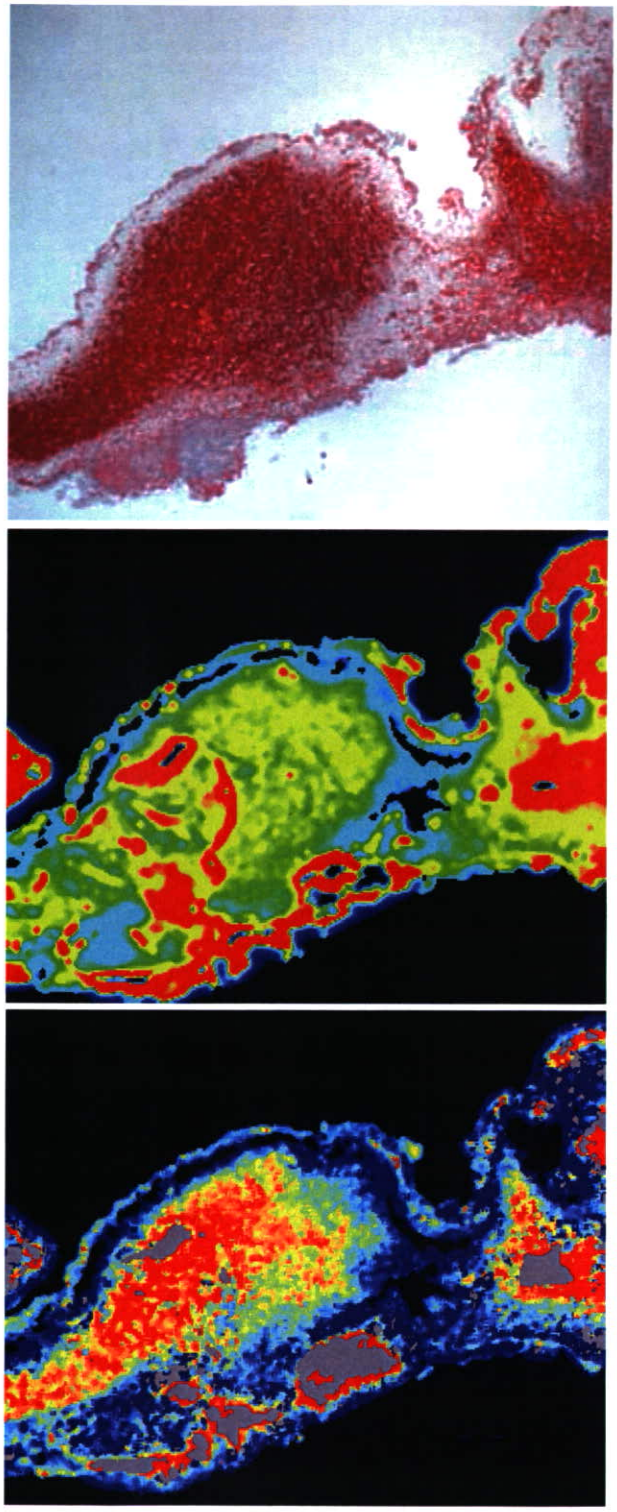

Figure 5. Optical (upper), attenuation (middle) and sound speed (lower) images of the thrombus 19 hours after AMI onset.

The values of attenuation constant and sound speed of the fresh red-thrombus were significantly higher than those of the fresh white-thrombus. Both parameters of red-thrombus decreased gradually after thrombus formation, and both parameters increased again with the organization with collagen fibers. Both parameters were high in the lesion of infiltration of inflammatory cells.

IV. Conclusion

The acoustic properties of thrombus at different stages of pathology can be classified by scanning acoustic microscopy. These criteria will provide a basis for the interpretation of conventional and VH-IVUS.

Acknowledgment

This study was supported by Grants-in-Aid for Scientific Research (Scientific Research (B) 13557059, 15300178) from the Japan Society for the Promotion of Science, Health and Labor Sciences Research Grants from the Ministry of Health, Labor and Welfare for the Research on Advanced Medical Technology (H17-Nano-001) and The Grant on Three Dimensional Organ Regeneration Program from New Energy and Industrial Technology Development Organization.

References

[1] Saijo Y, Jorgensen CS, Falk E. Ultrasonic tissue characterization of collagen in lipid-rich plaques in apoE-deficient mice. Atherosclerosis Vol. 158, No. 2; 289-295, 2001.

[2] Saijo Y, Ohashi T, Sasaki H, Sato M, Jorgensen CS, Nitta S. Application of scanning acoustic microscopy for assessing stress distribution in atherosclerotic plaque. Ann Biomed Eng, Vol. 29, No. 12, 1048-53, 2001.

[3] Sasaki H, Saijo Y, Tanaka M, Nitta S. Influence of tissue preparation on the acoustic properties of tissue sections at high frequencies. Ultrasound Med Biol, Vol. 29, No. 9, 1367-72, 2003.

[4] Hozumi N, Yamashita R, Lee CK, Nagao M, Kobayashi K, Saijo Y, Tanaka M, Tanaka N, Ohtsuki S. Time–frequency analysis for pulse driven ultrasonic microscopy for biological tissue characterization. Ultrasonics, Vol. 42, No. 1-9, 717-722, 2004.

[5] Saijo Y, Sasaki H, Hozumi N, Kobayashi K, Tanaka M, Yambe T. Sound speed scanning acoustic microscopy for biomedical applications. Technol Health Care. Vol. 13, No. 4: 261-7, 2005.

[6] Saijo Y, Hozumi N, Lee C, Nagao M, Kobayashi K, Oakada N, Tanaka N, Santos Filho ED, Sasaki H, Tanaka M, Yambe T. Ultrasonic speed microscopy for imaging of coronary artery. Ultrasonics. 2006 Jul 3; [Epub ahead of print]

Tissue Sound Speed of Anterior Cruciate Ligament in Estrogen-Controlled Rabbits

- A Measurement using the Scanning Acoustic Microscope -

Hirotaka Sano, MD[1)], Koshi Hattori, MD[1)], Tatsuro Komatsuda, MD[2)], Yoshifumi Saijo, MD[4)], Takehiko Sugita[3)], MD and Eiji Itoi, MD[1)]
Departments of Orthopaedic Surgery, Tohoku University School of Medicine[1)], Tohoku Rosai Hospital[2)] and Honma Memorial Tohoku Orthopaedic Hospital[3)]
Department of Medical Engineering and Cardiology, Institute of Development, Aging and Cancer, Tohoku University[4)]
Sendai, Japan
Corresponding author: Hirotaka Sano, MD, E-mail: staka@mail.tains.tohoku.ac.jp

Abstract— To elucidate the pathogenetic roles of estrogen in the rupture of anterior cruciate ligament (ACL), the hormonal effects of estrogen on the material properties of ACL tissue should be fully clarified.

In 40 ovariectomized Japanese white rabbits, serum estrogen level was controlled by the intramuscular injection of estradiol. They were divided into 4 groups according to the dose of administered estradiol (Groups L, M, H and C). Intramuscular injection of 17β-estradiol was performed 1, 2, 3 and 4 weeks after surgery with the doses in Groups L, M, and H were 50, 100, and 500 μg/kg. For Group C, which served as control, no estradiol was administered. After 5 weeks from the overiectomy, lateral portion of ACL was harvested and fixed with 10% neutralized formalin and embedded in paraffin. The specimens were cut perpendicularly to the ligament fibers in the thickness of 10 μm both for routine histologic staining and SAM measurement.

In the measurement of SAM, Group M indicated the lowest value of tissue sound speed among 4 groups, which could be interpreted as the lowest Young's modulus. A statistically significant difference was found in the tissue sound speed between Groups C and M ($p=0.028$). We assumed that estrogen might constitute one of the pathogenetic factors of the ACL ruptures in the female athletes.

Keywords- anterior cruciate ligament, rupture, female, sound speed, scanning acoustic microscope

I. Introduction

Previous epidemiologic studies revealed that the ruptures of anterior cruciate ligament (ACL) were more frequently seen in female athletes than in male athletes [10]. In 1997, Bjordal reported that the ACL rupture rate in female soccer players was almost twice as high as that in males [1]. Among high school basketball players, the incidence of ACL rupture was reported as more than three times higher in female athletes than in male athletes [8].

To explain this sex difference, a number of pathogenetic factors have been proposed including lower limb alignment, shape of the intercondylar notch, joint laxity, hormonal effects, ligament size and body weight, etc [2], [3], [5], [16], [19]. However, the principal pathogenetic factor for the sex difference still remains unclear.

Given these controversies, the authors developed an estrogen-controlled rabbit model to clarify the hormonal effects of estrogen on tissue material property of ACL [4]. In this model, all animals were ovariectomized and then divided into 4 groups according to the administrated dose of estradiol. In the current study, we measured the tissue sound speed of their ACL, which closely correlates to their Young's modulus, using a scanning acoustic microscope (SAM). The purpose of this study was to compare the tissue sound speed between these 4 animal groups.

II. Materials and Methods

Animal model

The experimental procedures were approved by the committee for animal experimentation, Tohoku University School of Medicine.

Forty age-matched female Japanese white rabbits (32 weeks old) were used for the current project. Their average body weight was 4.3 (SD 0.43) kg. All were ovariectomized under general anesthesia using an intramuscular injection of ketamine hydrochloride (0.5 mg/kg) and xylazine (1.0 mg/kg). Each rabbit was housed in a cage individually under the same conditions, including room temperature, humidity, food and water. To prevent postoperative infection, enrofloxacin (5 mg/kg) was injected once a day into the back muscle for 3 days postoperatively.

The animals were divided into 4 groups (10 in each group) according to the dose of administered estradiol (low, medium, high and control: L, M, H and C). One rabbit in Group M died due to an anesthetic problem during surgery, thus this animal was excluded from analysis. In the other 39 rabbits, no postoperative infections were seen. Intramuscular injection of 17β-estradiol (Ovahormon depot®, Teikoku Hormone Manufacturing Co., Ltd. Japan) was performed 1, 2, 3 and 4 weeks after surgery. The doses of 17β-estradiol in Groups L, M, and H were 50, 100, and 500 μg/kg. For Group C, which served as control, neither estradiol nor any types of vehicles were administered.

Preparation of the specimens

All rabbits were killed with an overdose of pentobarbital sodium 5 weeks after the ovariectomy. The right hind limb was disarticulated at the hip, and the knees were dissected to expose the ACL. The ACL was divided into the lateral (lACL) and the medial portions (mACL). The femur-mACL-tibia complex was used for the biomechanical testing in our previous study [4], whereas lACLs were used for the current study. The specimens of lACL were fixed in 10% neutralized formalin and embedded in paraffin. Then, they were cut perpendicularly to the ligament fibers in the thickness of 10μm. Serial sections were made both for the SAM measurements and routine histologic staining including haematoxylin-eosin and elastica-Masson.

Measurement of the tissue sound speed of the lACL

A SAM system specially developed in Tohoku University, operating in the frequency range of 50-150 MHz, was used for this study [11-15]. The sections for SAM measurements were mounted on glass slides but not covered by cover slips. The paraffin was removed from the sections by the graded alcohol method prior to the ultrasonic measurement. Distilled water was used as the coupling medium, which maintained the specimen at 20°C during the measurement procedure. A single ultrasound pulse of 5 ns width was emitted and received by the same transducer above the specimen. The reflections from the tissue surface and those from the interface between the tissue and glass were introduced into a digital oscilloscope. Four values of the time taken for a pulse response at the same point were averaged in the oscilloscope in order to reduce the noise in the measurement. The transducer was mounted on an X-Y stage with a microcomputer board that was driven by the computer installed in the digital oscilloscope. The X-scan was driven by a linear servo motor, and the Y-scan was driven by a stepping motor. The area of measurement was 2.4 × 2.4 mm (300 × 300 pixels).

It is known that tissue sound speed is directory proportional to the square root of its Young's modulus as following equation shows,

$$c = \sqrt{\frac{E(1-\sigma)}{\rho(1+\sigma)(1-2\sigma)}}$$

(c: sound speed, E: Young's modulus, ρ: density, σ: Poisson's ratio).

To measure the tissue sound speed, SAM system required to look up three reflection data directory from the glass surface. Thus, three reference points without lACL tissue were determined manually on the monitor. Then, a two-dimensional distribution of sound speed in a specimen was displayed and saved as an image file using a color-coded scale. A gray scale image was also saved as an image file for further quantification of the tissue sound speed.

Quantification of tissue sound speed of ACL

To exclude the artifacts caused during the cutting process, the area where ligament tissue was properly transected was determined histologically as the region of interest (ROI). In each specimen, a gray-scale image was imported to the commercial software, Adobe Photoshop (version 7.0). With this image, the average value of density (between 0 and 255) of ROI was measured 5 times using the analysis option, "histogram". Then, the mean value of these 5 measurements (*mean density*) in each specimen was converted again to the sound speed (*mean sound speed*). Then, the *mean sound speed* was compared between the 4 animal groups to find out whether estrogen altered tissue elasticity of lACL or not.

Statistical analyses

Statview 5.0 (SAS Institute Inc.) was used for the statistical analyses in the current study. The Dunnett T3 test was used to determine the differences in the tissue sound speed among 4 animal groups. Differences were considered as statistically significant when the p-value was less than 0.05.

III. Results

A two-dimensional distribution of the tissue sound speed was successfully measured with SAM (**Figure 1**). All 3 estrogen-administrated animal groups (Groups L, M and H) indicated lower sound speed than that of Controls (Group C). Especially, Group M indicated the lowest value of the tissue sound speed among 4 groups, which could be interpreted as the lowest Young's modulus. A statistically significant difference was found in the tissue sound speed between Groups C and M ($p=0.028$, **Table 1**).

IV. Discussion

The pathogenetic roles of estrogen in ACL ruptures have not been fully clarified yet. Controversies still continues whether estrogen alters the mechanical properties of the ACL tissue or not. In 1997, Liu et al. reported that the presence of estrogen receptors was evident in the nuclei of synoviocytes, fibroblasts and cells in the blood vessel walls in ACL. They concluded that estrogen had some effects on both the cell composition and the histological structure [7]. Slauterbeck et al. investigated the relationship between the administrated dose of estrogen and the mechanical properties of the ACL using the ovariectomized rabbit model. They concluded that estrogen might alter the biomechanical strength of ACL [17]. More recently, Wojtys et al. reported that the incidence of ACL ruptures in the female athletes was closely correlated to the menstrual cycle [20]. All these findings supported the hypothesis that estrogen plays an important role in the ACL ruptures of female athletes. On the other hand, both Strickland et al. [18] and Rau et al. [9] reported that estrogen might not alter the material properties of ACL, especially within normal physiological range.

Based on these controversies, the authors tested biomechanical strength of femur-mACL-tibia complex in the estrogen-controlled rabbit models in our previous study. However, no significant differences in the ultimate tensile stress were found between any estradiol-administered group and Group C [4]. In the conventional biomechanical testing procedure, the femur-mACL-tibia complex was tested as one unit. Failure was occurred at the insertion in all specimens during the tensile testing. We assumed that the ultimate tensile stress measured in this study might not be directory reflected the alteration in the collagen fibers of ACL.

Since the estrogen receptors were localized in the ligament proper (i.e., nuclei of synoviocytes, fibroblasts and cells in the blood vessel walls) [6], the tissue elasticity of ligament proper should be measured at a microscopic level to clarify the direct effects of estrogen on ACL. Thus, in the current study, we focused on the ligament proper of lACLs and measured their elasticity using SAM. Our results clearly demonstrated that all 3 estradiol-administered groups showed lower sound speed than that of Group C. Moreover, a significant difference in the tissue sound speed was seen between Groups M and C. In other words, the ligament proper of Group M indicated the softest material property among 4 animal groups.

Based on these results, we assumed that estrogen might constitute one of the pathogenetic factors of the ACL ruptures in the female athletes. Further studies with lager number of animals will be needed to clarify the dose-dependent relationship between estrogen and the material properties of ACL.

V. Acknowledgments

The authors thank Mr. Katsuyoshi Shoji, Ms. Michiko Fukuyama in the Department of Orthopaedic Surgery, Tohoku University School of Medicine for their technical assistance.

Figure 1-a, b, c: Typical two-dimensional distribution pattern of tissue sound speed in lACL (Sample No.40-2, Group H).

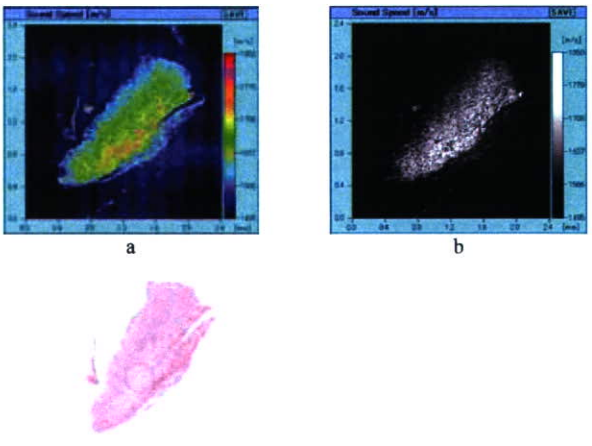

a: SAM image with a color-coded scale, b: SAM image with a gray scale, c: haematoxylin-eosin staining (The circular area indicates the region of interest).

Table 1: Mean tissue sound speed and SD of lACLs in 4 animal groups

	Group C	Group L	Group M	Group H
Mean sound speed (m/s)	1727	1683	1665*	1690
SD	32	53	63	56

All three estrogen-administrated groups (Groups L, M and H) represented lower sound speed than that of Group C (Controls). A statistically significant difference was found between Group C and Group M (*p=0.028).

REFERENCES

[1] J.M. Bjordal, F. Arnly, B. Hannestad, T. Strand, Epidemiology of anterior cruciate ligament injuries in soccer. Am. J. Sports Med., **25** (1997) 341-345.

[2] T.G. Grace, E.R. Sweetser, M.A. Nelson, L.R. Ydens, B.J. Skipper, Isokinetic muscle imbalance and knee-joint injuries. A prospective blind study. J. Bone Joint Surg. (Am) **66** (1984) 734-740.

[3] M.R. Hutchinson, M.L. Ireland, Knee injuries in female athletes, Sports Med. **19** (1995) 288-302.

[4] T. Komatsuda, H. Sano, Does estrogen alter the mechanical properties of the anterior cruciate ligament ? Acta Orthop Scand, *in press*.

[5] A.S. Levy, M.J. Wetzler, M. Lewars, W. Laughlin, Knee injuries in women collegiate rugby players. Am. J. Sports Med., **25** (1997) 360-362.

[6] S.H. Liu, R.A. Al-Shaikh, V. Panossian, R.S. Yang, S.D. Nelson, N. Soleiman, G.A. Finerman, J.M. Lane, Primary immunolocalization of estrogen and progesterone target cells in the human anterior cruciate ligament. J. Orthop. Res., **14** (1996) 526-533.

[7] S.H. Liu, R.A. Al-Shaikh, V. Panossian, G.A. Finerman, J.M. Lane, Estrogen affects the cellular metabolism of the anterior cruciate ligament. A potential explanation for female athletic injury. Am. J. Sports Med., **25** (1997) 704-709.

[8] D.F. Messina, W.C. Farney, J.C. DeLee, The incidence of injury in Texas high school basketball. A prospective study among male and female athletes. Am. J. Sports Med., **27** (1999) 294-299.

[9] M.D. Rau, D. Renouf, D. Benfield, D.D. Otto, G.M. Thornton, V.J. Raso, K.M. Bagnall, Examination of the failure properties of the anterior cruciate ligament during the estrous cycle. Knee, **12** (2005) 37-40.

[10] H. Roos, M. Ornell, P. Gärdsell, L.S. Lohmander, A. Lindstrand, Soccer after anterior crusiate ligament injury – an incompatible combination? A national survey of incidence and risk factors and a 7-year follow-up of 310players. Acta Orthop. Scand., **66**, (1995) 107-112.

[11] Y. Saijo, H. Sasaki, H. Okawai, D. Nagamura, M. Tanaka, Acoustic Properties of the Normal and Pathologic Myocardium by Scanning Acoustic Microscopy. Jpn J. Med. Ultrasonics, **22** (1995) 29-40.

[12] Y. Saijo, H. Okawai, H. Sasaki, S. Masaaki, C.S. Jorgensen, S. Nitta, Application of Acoustic Microscopy for Assessing Stress Disrtribution in Atherosclerotic Plaque. Ann. Biomed. Eng., **29** (2001) 1048-1053.

[13] Y. Saijo, H. Sasaki, N. Hozumi, K. Kobayashi, M. Tanaka, T. Yambe, Sound speed scanning acoustic microscopy for biomedical applications. Technol. Health Care, **13** (2005) 261-267.

[14] Y. Saijo, C.S. Jorgensen, E. Falk, Ultrasonic tissue characterization of collagen in lipid-rich plaques in apoE-deficient mice. Atherosclerosis, **158** (2001) 289-295.

[15] Y. Saijo, M. Tanaka, H. Okawai, H. Sasaki, S.I. Nitta, F. Dunn, Ultrasonic tissue characterization of infarcted myocardium by scanning acoustic microscopy. Ultrasound Med. Biol., **23** (1997) 77-85.

[16] P. Schantz, E. Randall-Fox, W. Hutchison, A. Tyden, P.O. Astrand, Muscle fibre type distribution, muscle cross-sectional area and maximal voluntary strength in humans. Acta Physiol. Scand., **117** (1983) 219-226.

[17] J. Slauterbeck, C. Clevenger, W. Lundberg, D.M. Burchfield, Estrogen level alters the failure load of the rabbit anterior cruciate ligament. J. Orthop. Res., **17** (1999) 405-408.

[18] S.M. Strickland, T.W. Belknap, S.A. Turner, T.M. Wright, J.A. Hannafin, Lack of hormonal influences on mechanical properties of sheep knee ligaments. Am. J. Sports Med., **31** (2003) 210-215.

[19] E.M. Wojtys, L.J. Huston, T.N. Lindenfeld, T.E. Hewett, M.L. Greenfield, Association between the menstrual cycle and anterior cruciate ligament injuries in female athletes. Am. J. Sports Med., **26** (1998) 614-619.

[20] E.M. Wojtys, L.J. Huston, M.D. Boynton, K.P. Spindler, T.N. Lindenfeld, The effect of the menstrual cycle on anterior cruciate ligament injuries in women as determined by hormone levels. Am. J. Sports Med., **30** (2002) 182-188.

Image Processing for Scanning Type Biological Ultrasonic Microscope Considering Its Beam Characteristics

K. Kobayashi T.Ishiguro
Honda Electronics Co., Ltd.
Toyohashi, Japan

Y. Saijo
Tohoku Univ.
Sendai, Japan

N.Hozumi
Aichi Inst. of Technology
Toyota, Japan

Abstract— **We have been developing a biological ultrasonic microscope with a high lateral resolution.**
An acoustic pulse is transmitted by a scanning transducer to a substrate on which a thin slice of a tissue is embedded. The transducer has a minute curvature in order to focus an acoustic beam with a high frequency component. It may be fabricated by MEMS technology; however from the point of view of engineering, it may not be easy to guarantee the reproducibility of beam pattern as specified. In a high frequency range, a small error in fabrication will lead to a big difference in beam pattern which strongly affects the observed image. Using newly proposed methodology to observe a well-defined pin-hole, we found that each commercial single probe transducer with the same specification has a unique beam pattern. In addition, the pattern was not always concentric. Consequently, we proposed a method to compensate the image that was obtained using an eccentric beam pattern. A clearer image was successfully obtained after the compensation.A clearer image was successfully obtained after the compensation.
Keywords: biological tissue; beam form; micro-scale imaging.

I. INTRODUCTION

Pulse excitation ultrasonic sound-speed microscopes are useful as the quantitative evaluation equipment for tissue sound-speed. They use pulse waves for measurement of tissue sound-speed, and therefore use polymer transducers to achieve highly sensitive measurements with the pulse waves. To make a focused transducer using polymer piezoelectric film, the film is adhered to a metal bar that is processed to be concave according to the focal length. Sometimes the ideal focus cannot be made due to thickness of adhesive and film creases. It is impossible to generate polymer transducers for 100 MHz or higher frequencies, and the current pulse excitation ultrasonic sound-speed microscopes use transducers of 80 MHz and have a resolution of 18 μm. In pathology departments where tissue observations are implemented, optical microscopes are generally used. It is difficult to determine tissue structures in ultrasonic images with a resolution of 18 μm, because the resolution differs from that of commonly used optical microscopes. To solve this, we measured directional properties of the ultrasonic transducer and used them for improvement of blurred images. The improvement method is reported below.

II. PRINCIPLE

When an image is created by sending and receiving ultrasonic waves with an ultrasonic microscope, the resultant image is more unclear than the actual structure, as shown in Figure-1, due to directional properties of the ultrasonic transducer. The unclear image is an image obtained by applying the directional property function of the transducer to the true structure as a transfer function.

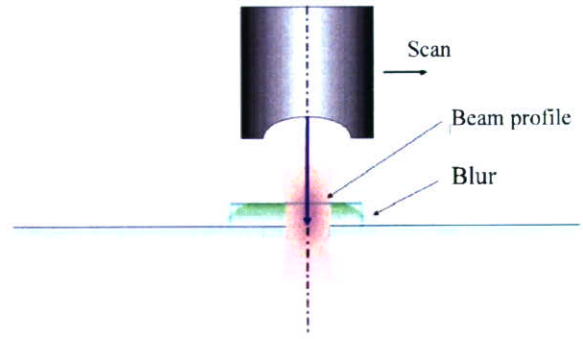

Figure-1 Blur under an ultrasonic microscope

When this blur is captured one-dimensionally, it is expressed as shown in Figure-2; where the true value is convolved by the transfer characteristic H.

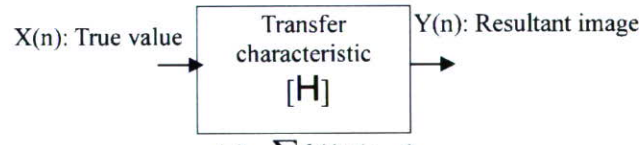

Figure-2 Mechanism of blur

When this is considered two-dimensionally, the relationship between the true acoustic intensity image and the actually observed acoustic intensity image is expressed as:

$$\text{actual}(x, y) = \iint h(u, v)\,\text{ideal}(x-u, y-v)\,du\,dv$$
$$= h(x,y) * \text{ideal}(x,y) \quad (1)$$

ideal(x, y) : True acoustic intensity image
actual(x, y) : Actually observed acoustic intensity image
h(x, y) : Transfer function of the observation system
(* indicates convolution.)

When a focus is made at a point on the view plane in sending and receiving ultrasonic waves, the transfer function becomes a delta function,

$$h(x, y) = \delta(x, y) = 1 \{x = 0, y = 0\}$$
$$0 \{ \text{ else } \}$$

$$\text{actual}(x, y) = \text{ideal}(x, y)$$

and the observed acoustic intensity image accords with the true acoustic intensity image. On the other hand, when a focus is not made at a point but spreads on the view plane, the transfer function has the frequency dependency and has a characteristic that signals are more attenuated as the frequency becomes higher. As a result, the observed image becomes blurred and becomes different from the true image. Though the signal components are attenuated at higher frequencies, they will not be lost completely.

By applying the Fourier transform to equation (1), derive the relationship in the frequency domain as follows:

$$ACTUAL(\omega x, \omega y)=(\omega x, \omega y) \bullet IDEAL(\omega x, \omega y) \quad (2)$$

$$IDEAL(\omega x, \omega y) = FT\{ideal(x, y)\}$$
$$ACTUAL(\omega x, \omega y) = FT\{actual(x, y)\}$$
$$H(\omega x, \omega y) = FT\{h(x, y)\}$$

(FT{} indicates the Fourier transform in {}.)

This transforms the convolution relationship in equation (1) to a simple product relationship in equation (2). This way, restoration of the true image from an observed image in the frequency domain is expressed by the following formula, and an image in the actual image domain can be obtained through the inverse Fourier transform of the result.

$$IDEAL(\omega x, \omega y)= \{1/H(\omega x, \omega y)\} \bullet ACTUAL(\omega x, \omega y) \quad (3)$$

$$ideal(x, y) = IFT\{IDEAL(\omega x, \omega y)\}$$

(IFT{} indicates the inverse Fourier transform in {}.)

Restoration requires the reverse characteristic of the transfer characteristic. Using a sample from which the true image can be assumed, determine the reverse characteristic from the assumed image and the actually observed image in advance.

$$\{1/H(\omega x, \omega y)\} = IDEAL\_ref(\omega x, \omega y)/ACTUAL\_ref(\omega x, \omega y) \quad (4)$$

$$IDEAL\_ref(\omega x, \omega y) = FT\{ideal\_ref(x, y)\}$$
$$ACTUAL\_ref(\omega x, \omega y) = FT\{actual\_ref(x, y)\}$$

To be exact, it is necessary to determine equation (4) in consideration of not only the amplitude information but also the phase information (as a complex number). But the blur characteristic is almost symmetric about a point, so determine equation (4) simply as an amplitude spectrum ratio, disregarding the phase information.

$$\{1/H(\omega x, \omega y)\} = Amp\{IDEAL\_ref(\omega x, \omega y)\}/Amp\{ACTUAL\_ref(\omega x, \omega y)\} \quad (5)$$

(Amp indicates the amplitude component in {}.)

The reverse characteristic is obtained as a scalar value, and can be handled as a simple restoration gain table in equation (3).

III. SAMPLE USED FOR REFERENCE

As a reference for determining the restoration gain table, we used a metal sample through which a pinhole of a diameter of 200 μm passes as shown in Figure-3 (a). From the data measured under an optical microscope, we assumed the true image on the assumption that the acoustic intensity in the pinhole is zero (0) and the acoustic intensity in parts other than the pinhole is uniform and equal to the average acoustic intensity in a part sufficiently away from the pinhole in the actually observed image. Figure-4 (b) shows an image actually observed under an ultrasonic microscope.

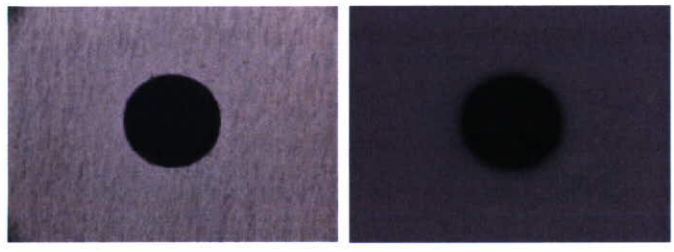

(a) Optical image (b) Ultrasonic image

Figure-3 Optical image and ultrasonic image of the reference of hole

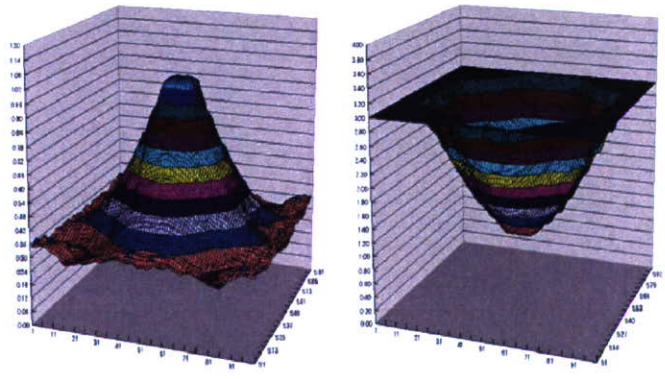

(a) Frequency characteristic of blur (b) Frequency characteristic of restoration

Figure -4 Frequency characteristic of blur and frequency characteristic of restoration

IV. LIMITATION OF RESTORATION GAIN TABLE

The transfer function of blur has a characteristic that signal components are more attenuated at higher frequencies as shown in Figure-4 (a). On the other hand, the restoration gain table becomes larger at higher frequencies. However, it is impossible to completely prevent entry of noise in actual acoustic intensity measurements, and it is necessary to limit the restoration gain table value. Otherwise, the effort to restore attenuated signals has the opposite effect of emphasizing noise components and deteriorating the image quality.

The evaluation on the observed image of the pinhole sample used for reference indicates that the noise components are equal to or higher than the signal components in the bands where the signal components are reduced to 1/5 or lower due to blur. Based on this result, we also assumed entry of more noises, and limited the restoration gain table value to three times as shown in Figure-4 (b).

V. RESULT

Figure-5 shows the result of restoring the ultrasonic observation image of a hole used for reference by utilizing the measured blur function. Figure-6 shows the restored image of a material with a circle of about 130 μm diameter around the same 100 μm hole. The hole and surrounding circle could be resolved with a resolution of 18 μm and observed at 100 MHz.

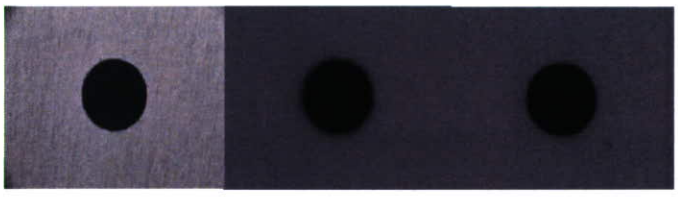

Figure-5 Improvement of the reference image

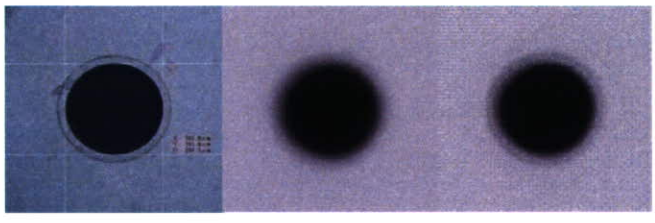

Figure-6 Improved image of a hole with link

When we treated observation examples of actual body tissues, we could eliminate blurs and obtain images close to optical images as shown in Figure-7 (esophagus), Figure-8 (mammary gland) and Figure-9 (stomach). These images were evaluated to be closer to optical images and easier to be judged in clinical use.

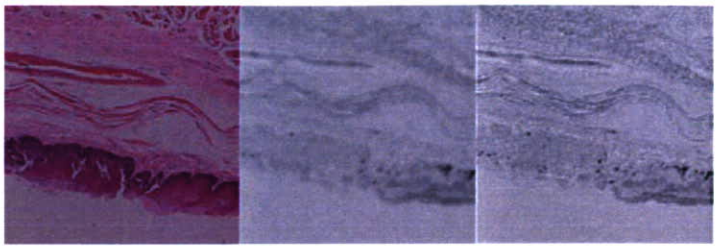

Figure-7 Improved image of body tissue (esophagus)

Figure-8 Improved image of body tissue

Figure-9 Improved image of body tissue (stomach)

VI. SUMMARY

Sharpening of images in consideration of the directional properties of transducer has been enabled by a simple arithmetic process by using the 2DFFT technique. It was found that high-resolution observation can be achieved without side-effects in actual observation by considering the SN when a reference image is captured and preventing noise from being included in determination of correction value. We will apply this method to high-frequency transducers for application in cell observation and other fields that require high resolution.

Non-mineralized fibrocartilage shows the lowest elastic modulus in the rabbit supraspinatus tendon insertion: Measurement with scanning acoustic microscopy

Hirotaka Sano, MD,[a] Yoshifumi Saijo, MD,[b] and Shoichi Kokubun, MD,[a] *Sendai, Japan*

The acoustic properties of rabbit supraspinatus tendon insertions were measured by scanning acoustic microscopy. After cutting parallel to the supraspinatus tendon fibers, specimens were fixed with 10% neutralized formalin, embedded in paraffin, and sectioned. Both the sound speed and the attenuation constant were measured at the insertion site. The 2-dimensional distribution of the sound speed and that of the attenuation constant were displayed with color-coded scales. The acoustic properties reflected both the histologic architecture and the collagen type. In the tendon proper and the non-mineralized fibrocartilage, the sound speed and attenuation constant gradually decreased as the predominant collagen type changed from I to II. In the mineralized fibrocartilage, they increased markedly with the mineralization of the fibrocartilaginous tissue. These results indicate that the non-mineralized fibrocartilage shows the lowest elastic modulus among 4 zones at the insertion site, which could be interpreted as an adaptation to various types of biomechanical stress. (J Shoulder Elbow Surg 2006;15:743-749.)

Previous clinical studies revealed that most of the rotator cuff tears were seen close to the insertion site of the supraspinatus tendon.[4,26] To elucidate the pathogenesis of the tendon tearing, both the histologic and the biomechanical characteristics of the insertion site should be fully clarified. Histologically, the supraspinatus tendon insertion consists of 4 zones, including the tendon proper, non-mineralized fibrocartilage, mineralized fibrocartilage, and bone.[5] This 4-zone structure constitutes a histologic transition from soft tissue (tendon) to bone. It is believed that the histologic transition at this site is accompanied by a change in the tissue material properties.[3,12] However, the actual material properties of the tendon insertion have not been measured yet because of its complicated histologic architecture. Recently, we developed finite element models of the supraspinatus tendon with its insertion.[22,27] Because no data was available for the material properties of fibrocartilage, medium values between the tendon and the cancellous bone were calculated and used for the analysis. The actual data of the material properties of fibrocartilage would improve the quality of these types of stress analyses.

Scanning acoustic microscopy (SAM) was first developed by Lemons and Quate in 1973[11] to visualize opaque materials at the microscopic level. Since then, we have been developing SAM for medicine and biology to measure tissue acoustic properties. It is known that tissue acoustic properties closely correlate to mechanical properties. Tissues representing heterogeneous histologic architecture could especially be assessed using SAM. In cardiology, SAM has already been applied for various types of soft tissues, that is, cardiac muscles, arterial plaques, vascular walls, etc.[16,17] On the other hand, the application of this technology in the orthopedic field has been limited to undecalcified bony specimens.[6,25] Recently, SAM was first applied to measure the acoustic properties of the supraspinatus tendon.[21] However, because this study only dealt with the tendon and not the 4-zone structure at its insertion, the transition of the tissue material properties still remains unclear.

Therefore, we attempted to describe the transition of the acoustic properties in the whole 4-zone structure at the insertion site of the rabbit supraspinatus tendon. We further attempted to determine the biomechanical characteristics of the supraspinatus tendon insertion.

MATERIALS AND METHODS

Preparation of the specimens

The supraspinatus tendon insertions of 3 Japanese white rabbits were used for the SAM measurement. They were all

From the [a]Department of the Orthopaedic Surgery, Tohoku University School of Medicine and [b]Department of Medical Engineering and Cardiology, Institute of Development, Aging and Cancer, Tohoku University.

Reprint requests to: Hirotaka Sano, MD, Department of Orthopaedic Surgery, Tohoku University, School of Medicine, 1-1 Seiryo-machi, Aoba-ku, Sendai, 980-8574, Japan (E-mail: *staka@mail.tains.tohoku.ac.jp*).

1058-2746/2006/$32.00
doi:10.1016/j.jse.2005.12.008

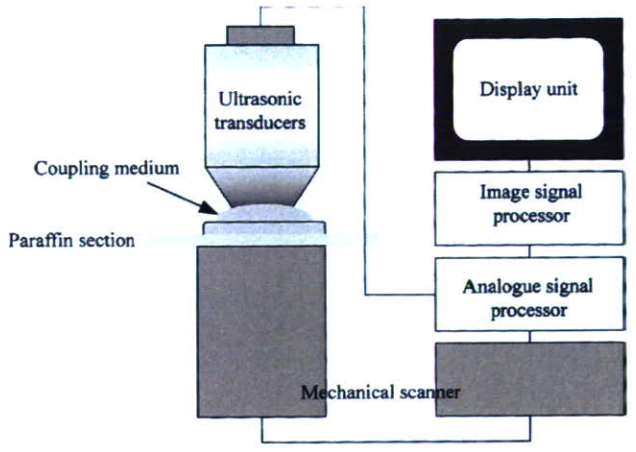

Figure 1 Block diagram of the system of the scanning acoustic microscopy.

6-month-old males, and their body weight was 3.2-3.5 kilograms. After euthanasia with an overdose of pentobarbital, bilateral supraspinatus tendons attached to the humeral heads were removed.

The specimens were cut parallel to the supraspinatus tendon fibers with a microcutting machine (EXAKT, Germany). The anterior parts of the supraspinatus tendons were fixed with 10% neutralized formalin for 12 hours. Because decalcification might alter the acoustic properties of the soft tissues, the humeral head was removed except for the insertion site to avoid decalcification. After embedding in paraffin, the specimens were cut at a thickness of 5 μm along the supraspinatus tendon fibers. Serial sections were made to compare the tissue acoustic properties to the histologic and the immunohistochemical characteristics.

Histologic investigations

Hematoxylin-eosin (HE) staining was routinely employed to assess the overall histologic structure. Immunohistochemical staining was also performed to confirm the presence of types I and II collagen at the insertion site. The avidin-biotinylated peroxidase complex method was employed using the monoclonal antibodies against types I and II collagens (anti-hCL(I) and anti-hCL(II), purified IgG, FUJI Chemical Industries Ltd., Toyama, Japan). Photographs were taken under the microscopy, and these were trimmed to create histologic images with areas identical to those of the SAM measurements.

SAM measurements

A specially developed SAM system, operating in the frequency range of 100-200 MHz, was employed for this study.[14,15] This system consists of 5 parts, viz. (1) ultrasonic transducers, (2) a mechanical scanner, (3) an analogue signal processor, (4) an image signal processor, and (5) a display unit (Figure 1). The focusing element is mechanically scanned at 60 Hz in a lateral direction (x) above the specimen, while the sample holder is scanned in the other lateral direction (y) for 8 seconds, thus providing 2-dimensional scanning. Images of the amplitude and phase are obtained in a 2-mm field of view. In the current study, we decided to focus on the articular surface of the supraspinatus tendon, because the entire width of the tendon could not be included in the single SAM measurement. Moreover, it has been known that the fibrocartilage is the most evident in the deep part of the tendon insertion but almost absent superficially.[3]

Distilled water was used as the coupling medium, which maintained the specimen at 20°C during the measurement procedure. The sections for SAM measurements were mounted on glass slides but not covered by coverslips. The paraffin was removed from the sections by the graded alcohol method prior to the ultrasonic measurement. Then, serial measurements were done with the SAM along the articular surface of the tendon from the insertion site to the musculotendinous junction. The data of the sound speed and the attenuation constant obtained were converted into color signals on the computer. Two-dimensional distribution patterns of those parameters were displayed and saved as an image file using color-coded scales. Then, these serial image files were connected together to reconstruct a single image from the insertion site to the musculotendinous junction.

The sound speed measured by SAM is defined by the following equation:

$$c = \sqrt{K/\rho} \qquad (1)$$

where c is the sound speed, K the elastic bulk modulus, and ρ the density. The relationship between the acoustics and a solid material can be described by modifying the above equation:

$$c = \sqrt{\frac{E(1-\sigma)}{\rho(1+\sigma)(1-2\sigma)}} \qquad (2)$$

where E is the Young's modulus and σ the Poisson's ratio. Equation 2 shows that the tissue sound speed, measured using SAM, is directly proportional to the square value of its Young's modulus.

RESULTS

Routine staining

The histologic specimens successfully included the area from the musculotendinous junction to the subchondral bone with the entire 4 zones of the insertion (Figure 2, a). In the tendon proper, the direction of the tendon fibers was longitudinal and nuclei were spindle shaped (fibroblasts). Although there was no distinct histologic border between the tendon proper and the non-mineralized fibrocartilage, the shapes of nuclei gradually changed to oval or round toward the non-mineralized fibrocartilage (chondrocytes). Between the non-mineralized and the mineralized fibrocartilage, there was a distinct blue line, the tidemark, seen histologically as a calcifying front (Figure 3, a).

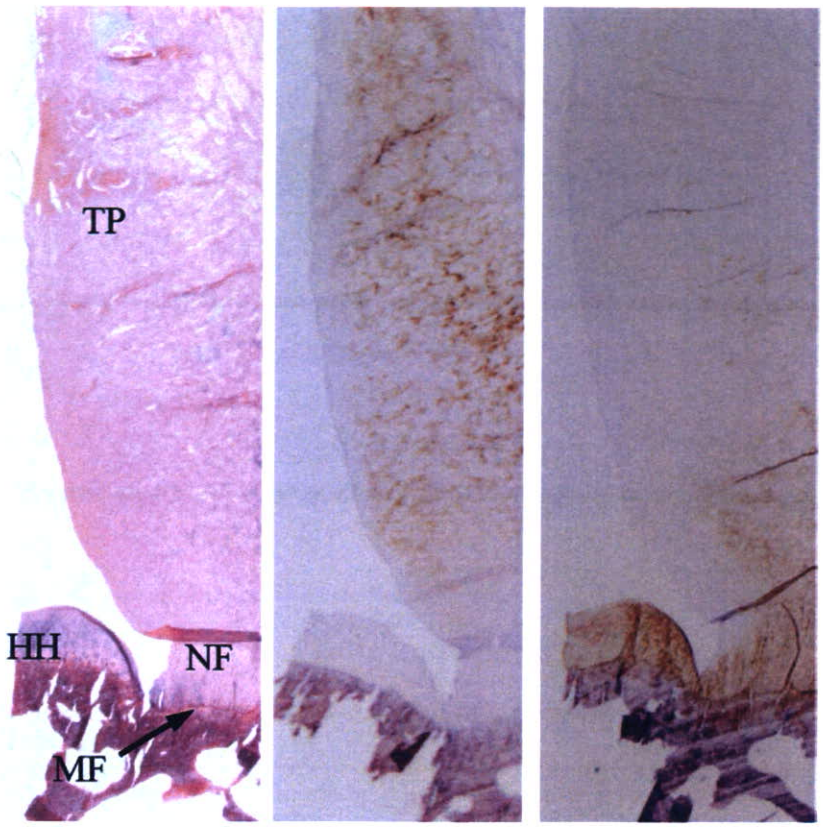

Figure 2 Histologic and immunohistochemical findings of the supraspinatus tendon and its insertion (Original magnification = ×1.25). (**a**) Hematoxylin-eosin; (**b**) type I collagen; (**c**) type II collagen. Type I collagen is positively stained in the tendon proper, whereas Type II collagen is localized in the fibrocartilage and the articular cartilage of humeral head. TP = tendon proper, NF = non-mineralized fibrocartilage, MF = mineralized fibrocartilage, HH = humeral head.

Collagen staining

Immunohistochemically, positive type I collagen was seen in the tendon proper. Between the tendon proper and the non-mineralized fibrocartilage, the predominant collagen type shifted from I to II (Figure 2, b, c). Type I collagen was not seen in the fibrocartilage (Figure 3, b). Additionally, both the non-mineralized fibrocartilage and the mineralized fibrocartilage were stained positively for type II collagen (Figure 3, c).

SAM measurements

The distribution of the sound speed and that of the attenuation constant showed almost identical patterns, which varied from zone to zone at the insertion (Figure 4, a, b). These 2 parameters reflected both the histologic architectures and the collagen types. In the tendon proper and the non-mineralized fibrocartilage, both the sound speed and the attenuation constant gradually decreased with the change in the predominant collagen type from I to II. The acoustic properties changed rapidly at the tidemark. In the mineralized fibrocartilage, they increased rapidly again with the mineralization of the fibrocartilaginous tissue (Figure 5, a, b). On the other hand, there were no differences in the acoustic properties between the mineralized fibrocartilage and the bone (Figure 5, a, b). The attenuation constant in both the mineralized fibrocartilage and the bone might have been beyond the upper limit of the SAM measurement. Table I summarizes the acoustic properties assessed in each zone.

DISCUSSION

There have been only a few reports published concerning the material properties of the supraspinatus tendon insertion.[7,13,20] In these studies, the entire bone-tendon complex was measured as one unit by conventional tensile testing procedures. More recently, Lee et al[10] measured the compressive stiffness of the human

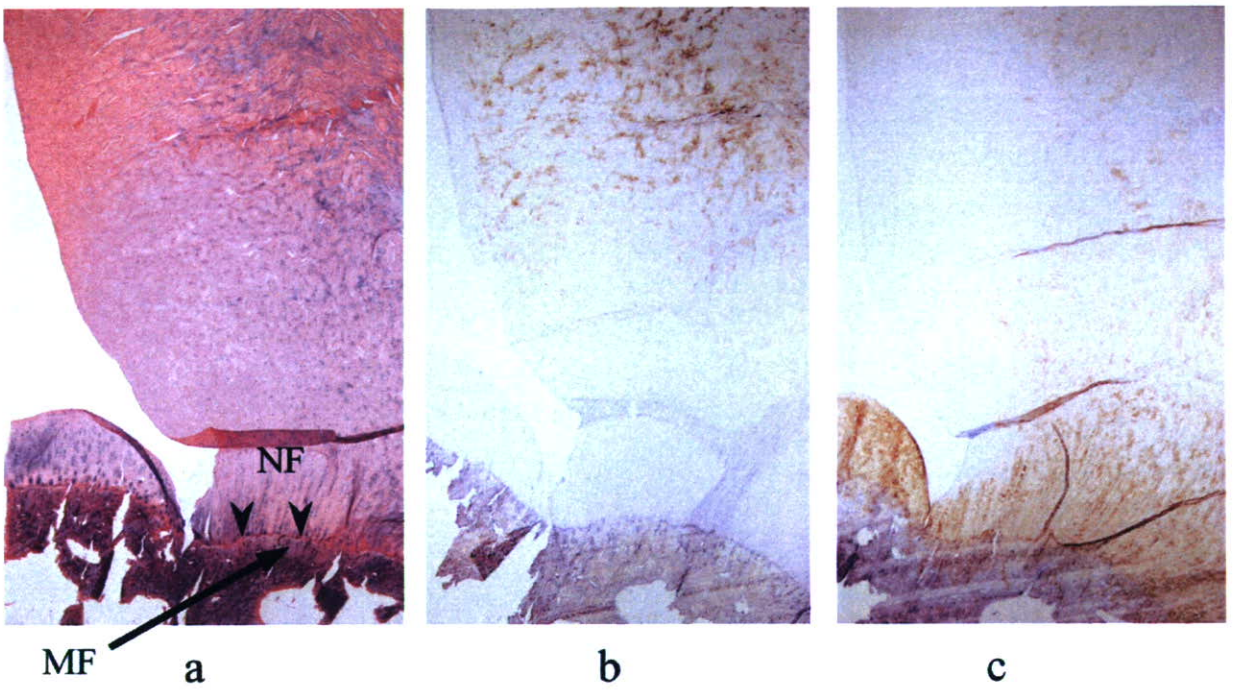

Figure 3 Higher magnification of the supraspinatus tendon insertion (Original magnification = ×4.00). (**a**) Hematoxylin-eosin; (**b**) type I collagen; (**c**) type II collagen. There is a distinct line (tidemark) between the non-mineralized fibrocartilage (NF) and the mineralized fibrocartilage (MF), which is a calcifying front (*arrowhead*). Both the non-mineralized and the mineralized fibrocartilage are positively stained with type II collagen.

supraspinatus tendon. Unfortunately, the insertion site was not included in their study. Thus, this is the first study measuring the material properties of each zone in the supraspinatus tendon insertion.

The advantages of applying SAM for such heterogeneous soft tissues are 3-fold. First, the material properties of each type of tissue can be measured non-destructively. Second, the preparation of specimens is simple, because only formalin-fixed paraffin sections are required. Such specimens can be used not only for routine histologic staining but also for immunohistochemical staining. Third, the distribution of the acoustic properties can be displayed in 2 dimensions. These 3 advantages enable a better understanding of the tissue material properties as well as comparisons with the histologic or the immunohistochemical characteristics.

The tissue sound speed measured with SAM was directly proportional to the square value of its Young's modulus (Equation 2). In other words, the sound speed (c) could be used as a parameter of the tissue material properties, especially the elasticity.[18] SAM also provides another acoustic parameter, the attenuation constant. Although the attenuation constant is not a pure physical parameter, it has a close relationship with the absorption of the ultrasound in the material.[18] The absorption by the tissue is known to be affected by its molecular weight and viscosity.[19] Moreover, the attenuation constant has a strong correlation with the sound speed. In the measurement of atherosclerotic human aorta with SAM, both the attenuation constant and the sound speed were lower in fatty plaque than in normal intima. On the other hand, both of them showed higher values in calcified plaques or fibrosis.[17]

In the current study, the acoustic properties corresponded well to the mineralization and the predominant collagen type. Accordingly, both the sound speed and the attenuation constant were the lowest in the non-mineralized fibrocartilage (type II collagen) among the 4 zones of the insertion site. Histologically, the direction of the tendon fibers was markedly changed at the non-mineralized fibrocartilage.[5] It was reported that the amount of non-mineralized fibrocartilage was greatest at sites where the change of the fiber angle was the most significant.[1,2] Moreover, recent finite element analysis revealed that the non-mineralized fibrocartilage is exposed not only to tensile force but also to compressive force.[27] Based on these findings, it was assumed that the non-mineralized fibrocartilage dissipates stress away from the insertion site.[9] We speculate that the variations in the Young's modulus at the insertion site may represent adaptations in response to biomechanical stress.

There were several limitations in the current study. First, the anatomy of the rabbit shoulder is different

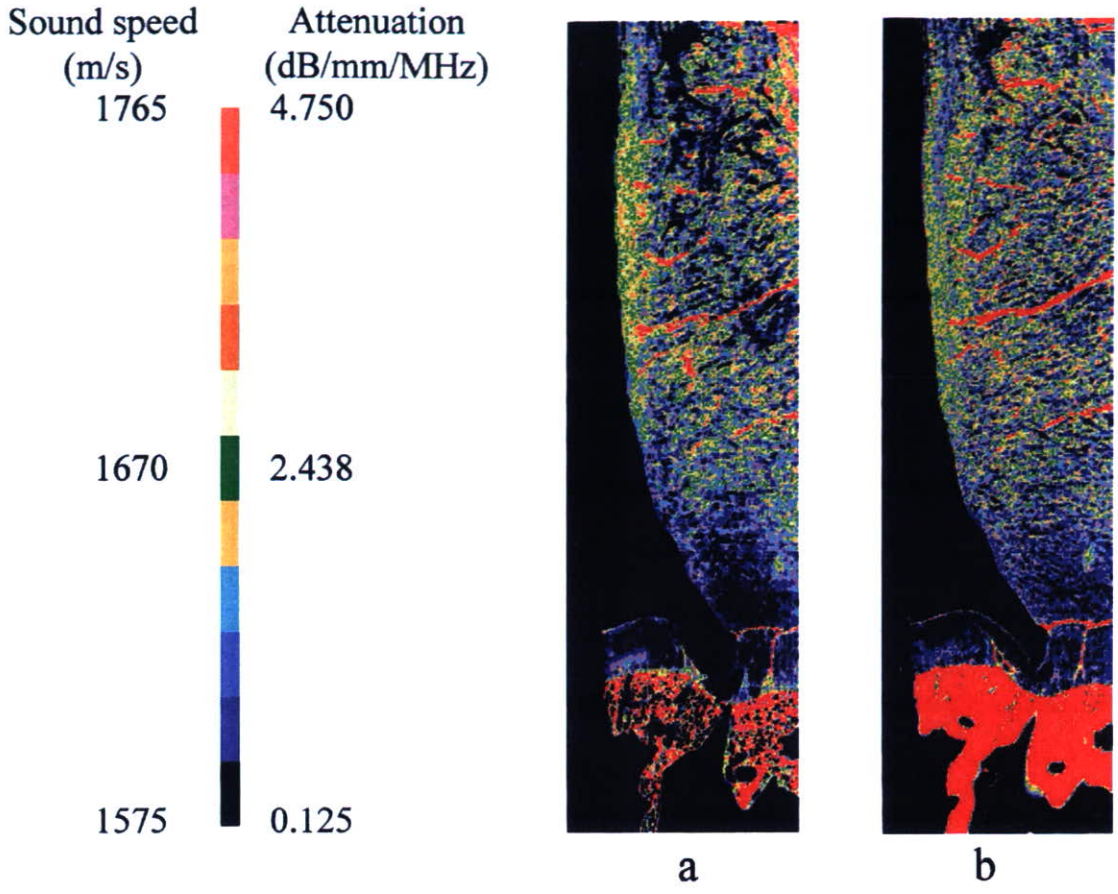

Figure 4 Two-dimensional distribution of the acoustic properties. (**a**) Sound speed; (**b**) attenuation constant. The 2-dimensional distribution of the sound speed and that of the attenuation constant show almost identical patterns. In the tendon proper and the non-mineralized fibrocartilage, these values gradually decrease with the change in the predominant collagen from type I to type II.

from that of humans.[24] Although the histologic structure of the rabbit supraspinatus tendon insertion is similar to that of humans,[8] its function differs. Second, the preparation of the tissue for SAM might alter the acoustic properties of the specimens, for example, formalin fixation, dehydration, paraffin embedding, etc. However, it has been already confirmed that such methods do not change significantly the tissue acoustic properties.[23] Thus, we believed that the relative relationships of the acoustic properties in the specimen would be preserved in the SAM measurement. Third, the Poisson's ratio and the density of the tissue should be measured at the microscopic level to determine the exact Young's modulus of the tissue.

The rabbit specimens measured in the current study did not exhibit any degenerative changes. In the clinical setting, partial thickness tears are frequently seen at the articular surface of the supraspinatus tendon insertion.[4] It has been thought that intrinsic degeneration is the primary pathogenetic factor in such partial thickness tears.[20,26] However, it is still unknown why degeneration occurs at this site. In the current study, we confirmed that the material properties of the supraspinatus tendon varied with the histologic characteristics. The elasticity of the tissue dramatically changed at the site of the tidemark, a calcifying front. Further investigations, including human specimens, would be needed to clarify the effects of the tissue material properties on the pathogenesis of degeneration and tendon tearing at the insertion site.

CONCLUSIONS

The acoustic properties of the supraspinatus tendon at the insertion were measured using SAM. Both the sound speed and the attenuation constant were the lowest in the non-mineralized fibrocartilage among the 4 zones of the insertion. These variations in the material properties at the insertion site could be interpreted as representing an adaptation to various types of biomechanical stress.

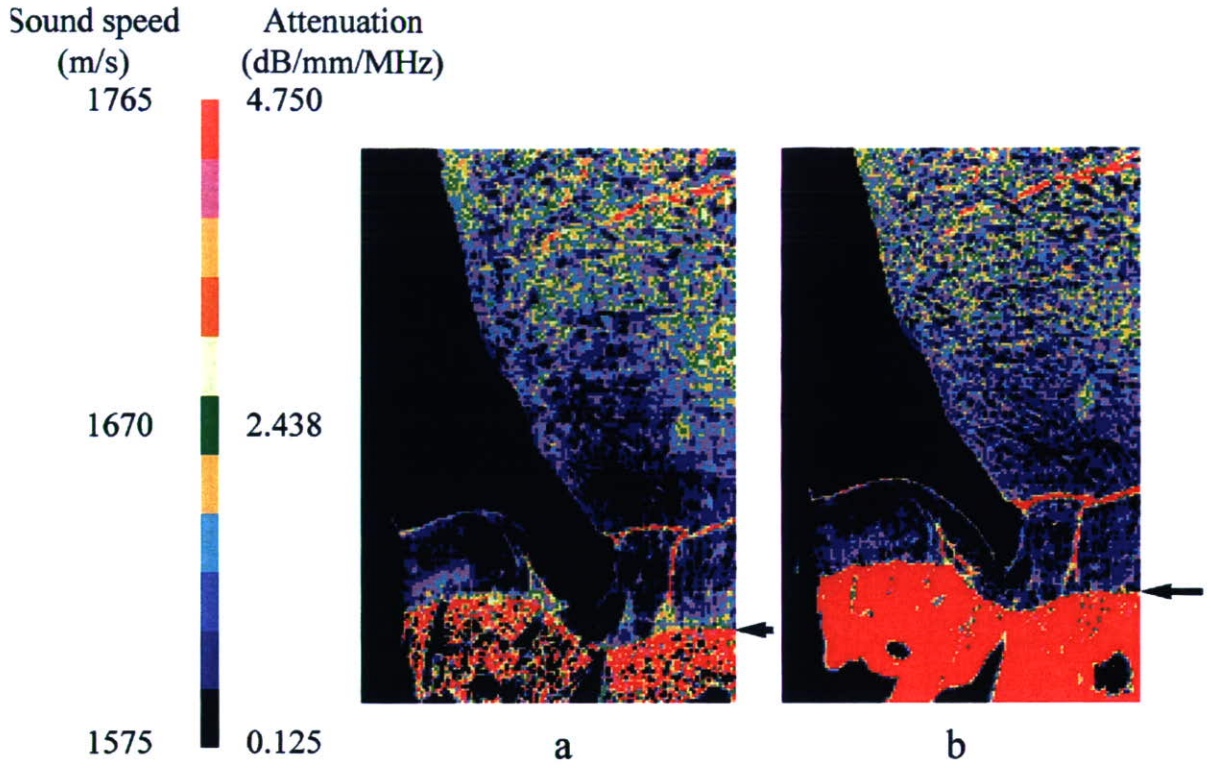

Figure 5 Acoustic properties at the supraspinatus tendon insertion. (**a**) Sound speed; (**b**) attenuation constant. The acoustic properties change dramatically at the tidemark (*arrow*). Both the sound speed and the attenuation constant indicate higher values in the mineralized fibrocartilage than in the non-mineralized fibrocartilage.

Table I The attenuation constant and the sound speed of each tissue at the supraspinatus tendon insertion

	Attenuation constant (dB/mm/MHz)	Sound speed (m/sec)
Tendon proper	2.225–3.065	1661–1695
Non-mineralized fibrocartilage	0.125–0.965	1575–1609
Mineralized fibrocartilage	4.330–4.750	1731–1765
Bone	4.330–4.750	1731–1765

REFERENCES

1. Benjamin M, Evans EJ, Rao RD, Findlay JA, Pemberton DJ. Quantitative differences in the histology of the attachment zones of the meniscal horns in the knee joint of man. J Anat 1991;177:127-34.
2. Benjamin M, Newell RLM, Evans EJ, Ralphs JR, Pemberton DJ. The structure of the insertions of the tendons of biceps brachii, triceps and brachialis in elderly dissecting room cadavers. J Anat 1992; 180:327-32.
3. Benjamin M, Ralphs JR. Fibrocartilage in tendons and ligament—an adaptation to compressive load. J Anat 1998,193: 481-94.
4. Codman EA. The shoulder. Boston, MA: Thomas Todd Company; 1934. p. 65–107.
5. Cooper RR, Misol S. Tendon and ligament insertion. A light and electron microscopic study. J Bone Joint Surg Am 1970;52A: 1-20.
6. Hasegawa K, Turner CH, Recker RR, Wu E, Burr DB. Elastic properties of osteoporotic bone measured by scanning acoustic microscopy. Bone 1995;16:85-90.
7. Itoi E, Berglund LJ, Grabowski JJ, et al. Tensile properties of the supraspinatus tendon. J Orthop Res 1995;13:578-84.
8. Kumagai J, Sarkar K, Uhlhoff HK, Okawara Y, Ooshima A. Immunohistochemical distribution of Type I, II and III collagens in the rabbit supraspinatus tendon insertion. J Anat 1994;185:279-84.
9. Kumai T, Takakura Y, Rufai A, Miltz S, Benjamin M. The functional anatomy of the human anterior talofibular ligament in relation to ankle sprains. J Anat 2002;200:457-65.
10. Lee S-B, Nakajima T, Luo Z-P, Zobitz ME, Chang Y-W, An K-N. The bursal and articular sides of the supraspinatus tendon have a different compressive stiffness. Clin Biomechanics 2000;15: 241-7.
11. Lemons RA, Quate CF. A scanning acoustic microscope. Proc IEEE Ultrasound Symp 1973:18-20.
12. Matyas JR, Anton MG, Shrive NG, Frank CB. Stress governs tissue phenotype at the femoral insertion of the rabbit insertion of the rabbit MCL. J Biomechanics 1995;28:147-57.
13. Nakajima T, Rokuuma N, Hamada K, Tomatsu T, Fukuda H. Histologic and biomechanical characteristics of the supraspinatus tendon: reference to rotator cuff tearing. J Shoulder Elbow Surg 1994;3:79-87.
14. Okawai H, Tanaka M, Chubachi N, Kushibiki J. Non-contact simultaneous measurement of thickness and acoustic properties of a biological tissue using focused wave in a scanning acoustic microscope. Jpn J Appl Physiol 1987;26:52-4.